Research Article

Modeling On-Body DTN Packet Routing Delay in the Presence of Postural Disconnections

Muhannad Quwaider,[1] Mahmoud Taghizadeh,[2] and Subir Biswas[2]

[1] *Department of Computer Engineering, Jordan University of Science and Technology, Irbid, Jordan 22110-3030, Jordan*
[2] *Department of Electrical and Computer Engineering, Michigan State University, East Lansing, MI 48824-1226, USA*

Correspondence should be addressed to Subir Biswas, sbiswas@egr.msu.edu

This paper presents a stochastic modeling framework for store-and-forward packet routing in Wireless Body Area Networks (*WBAN*) with postural partitioning. A prototype *WBANs* has been constructed for experimentally characterizing and capturing on-body topology disconnections in the presence of ultrashort range radio links, unpredictable RF attenuation, and human postural mobility. Delay modeling techniques for evaluating single-copy on-body DTN routing protocols are then developed. End-to-end routing delay for a series of protocols including opportunistic, randomized, and two other mechanisms that capture multiscale topological localities in human postural movements have been evaluated. Performance of the analyzed protocols are then evaluated experimentally and via simulation to compare with the results obtained from the developed model. Finally, a mechanism for evaluating the topological importance of individual on-body sensor nodes is developed. It is shown that such information can be used for selectively reducing the on-body sensor-count without substantially sacrificing the packet delivery delay.

1. Introduction

1.1. Body Area Networks. A number of tiny wireless sensors, strategically placed or implanted on a patient's body, can create a Wireless Body Area Network (*WBAN*) [1, 2]. A *WBAN* can monitor vital signs, providing real-time feedback for enabling many patient diagnostics procedures via continuous monitoring of chronic conditions, or recovery progress from an illness or surgical procedure. Data transaction across such sensors can be *point-to-point* or *multipoint-to-point*. While distributed detection of an athlete's posture [3, 4] would require *point-to-point* packet exchange across various on-body sensors, applications such as monitoring vital signs, as shown in Figure 1, will require all body-mounted and/or implanted sensors [2, 5] to route data *multipoint-to-point* to a sink node, which in turn can process and relay the information wirelessly to an out-of-body server. Data transaction can be also real-time or nonreal-time. While patient monitoring type of applications would require real-time packet routing, monitoring an athlete's physiological data can be collected offline for postprocessing

and analysis purposes. The routing protocols modeled in this paper cater to this *nonreal-time* class of on-body applications.

1.2. Short RF Range. In this paper we model on-body packet routing mechanisms in the presence of topological partitioning caused due to ultra-short wireless transmission range and postural body movements. Short transmission range is a common constraint for low-power RF transceivers designed for embedded applications with limited energy [6, 7], often supplied by harvested operations [8]. Such situations are particularly pertinent for implantable body sensors. Examples of ultralow range transceivers in the literature include [9] with 0-1 m, [8] with 0.2–1 m, [10] with 0.2 m, and [11] with 0-1 m transmission ranges. The corresponding transmission powers vary between 0.75 mW to 6 mW, which are within a range that can be handled with common harvesting techniques such as piezoelectric generation from body movements. Information available in the literature on such low power RF transceivers is summarized in Table 1.
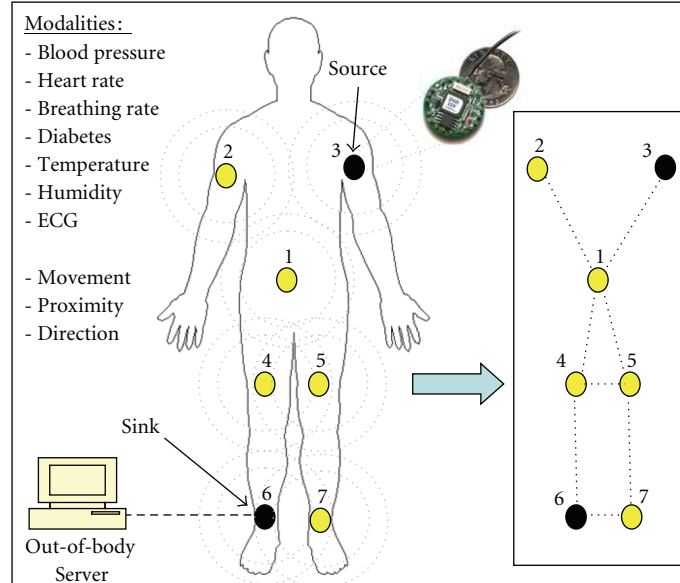
FIGURE 1: Body area sensor network.

TABLE 1: Low power and short range RF transceivers.

Reference	Tx Range (meter)	Tx. Power consumption (mWatt)	Rx. Power consumption (mWatt)
[8]	0.2–1	1.5–3.5	∼2.5
[9]	0-1	2	2
[10]	0.2	0.75–3.75	0.75–3.75
[11]	0-1	6	5.1

1.3. Routing with Network Partitioning. Low RF ranges also mean that postural body movements can give rise to frequent partitioning or disconnection in *WBAN* topologies, resulting in a body area Delay Tolerant Network (DTN) [12–17]. Such topological partitioning can often get aggravated by the unpredictable RF attenuation caused due to signal blockage by clothing material and body segments. Although real-time applications such as patient monitoring may not be supported in the presence of topological partitioning, nonreal-time applications such as athlete's physiology monitoring can still be supported using on-body DTN packet routing across disconnected partitions. Performance goals for such protocols will be to obtain (1) low end-to-end delay, (2) low packet loss, and (3) low transmission energy consumption.

1.4. Novelty and Contributions. The goal of this paper is to develop analytical modeling mechanisms for computing packet transfer delay for a series of DTN routing algorithms that can be implemented in an on-body setting. Although a number of papers in the literature [12–17] have studied DTN routing in general settings, to our knowledge, this is the first study that formally evaluates DTN routing delay in a *WBAN* through analytical model development. The dominating delay in DTN routing is contributed by packet buffering caused due to topological disconnections. In the absence of network congestions in low data-rate *WBANs*, such buffering delays are usually much larger compared to the congestion delay. That is why the congestion delay is not modeled in this paper. Specific contributions of the paper are as follows. First, we develop a prototype body area network for motivating the on-body packet routing problem and conducting on-body routing experiments with the DTN routing protocols that are modeled and evaluated in this paper. Second, a topology trace collection mechanism is developed for wirelessly extracting network topology, as a function of human postural dynamics, from the on-body sensors to an off-body server. Third, analytical techniques are developed for modeling the end-to-end packet delay for a range of DTN routing algorithms, namely, opportunistic [18–20] utility based [18, 20, 21], random [18, 20, 22], PRMPL [23, 24], and DVRPLC [23, 24]. Fourth, the DTN routing delays obtained from the developed model are compared with results from on-body experiments from the prototype WBAN and off-body simulation carried out on network topology traces obtained from the prototype WBAN. Finally, using the model and the topology trace data, a detailed analysis is carried out for identifying noncritical nodes in order to design a minimal WBAN topology from the routing stand point. The novelty of this approach includes (1) experimental evaluation of the proposed framework in a practical prototype *WBAN* system and (2) development of detailed delay models that can be useful for predeployment system dimensioning, planning, and what-if analysis of real body area networks.

2. Related Work

Most of the existing WBAN systems [1, 25–27] adopt star or tree topologies on a connected graph, leading to end-to-end

physical connectivity between any pair of on-body sensors at any given point in time. However, these models do not apply for the targeted DTN routing paradigm, which handles topology partitioning leading to scenarios in which end-to-end physical connectivity between node pairs may not be present all the time. Such partitioning is caused mainly due to the ultra short range RF transceivers as reported in Section 1.2.

The existing research on routing in Delay Tolerant Networks or DTNs is categorized [12, 13] as (1) replication based (multiple copy) [14, 17, 18] and (2) single copy [15, 19–21, 28]. The replication approach explores the ways in which several copies of a packet can be disseminated among several carrier mobile nodes to increase the chance of delivery to the desired destinations. Most of routing schemes proposed for DTN routing protocols belong to this category [17, 29–31]. While providing good delay performance, the primary limitation of these protocols is their energy and capacity overheads due to excessive packet transmissions. Further, under high traffic loads they may suffer from severe contention and subsequent packet drops that can degrade their performance and scalability [12, 13, 31, 32]. For ultraresource-constrained WBANs, such overheads are usually not acceptable. The single copy forwarding mechanisms make use of information about the connectivity and topology dynamics to make low-latency forwarding decisions with minimal replication overhead. The general principle is that when a node with a buffered packet encounters another node, the packet is forwarded to the encountered node only if it is more likely (than the node currently buffering the packet) to visit the destination node.

For the above mechanisms to work as anything beyond epidemic/viral routing [33], the nodes need to have certain degree of spatial and temporal locality in their mobility and meeting patterns. A notable DTN routing scheme in the literature is PROPHET [17] which is an extension of epidemic routing [29]. PROPHET develops a probabilistic framework for capturing the spatiotemporal locality present in the node mobility pattern within a dynamically partitioned wireless network. PROPHET can be implemented either in single copy or in multicope mode. Node interaction localities can be also captured in the form a per-link *utility* as detailed in [18, 19]. The link utility can be formulated as its age [19–21], formation frequency [19], and other historical parameters that can effectively capture the nodes' interaction localities.

Two additional routing protocols, namely, *opportunistic* [18–20] and *randomized* [19, 20], are also analyzed in the literature for applications in which either there is no node-interaction locality or such localities cannot be evaluated. With opportunistic routing, a source node directly delivers its packets to the destination node and buffers them till the link with the destination is formed. In randomized routing, packets are randomly routed following the hot-potato logic [20]. Both these protocols are hugely outperformed by the locality-based protocols [19, 20] due to their knowledge about the properties of the links.

In the existing literature, the above mechanisms are all applied to networks spanning across local to wide areas, few extending all the way up to the interplanetary scale [34], whereas in this paper the objective is to develop DTN routing for WBANs with ultra short transmission range. Also, the treated node mobility patterns in the literature are generally very different from what is observed for on-body DTN networks. The key objective of this work is to model the delivery delay of a number of representative DTN routing protocols, as identified above, in WBAN settings.

In [18, 19] the delay performance of single- and multi-copy DTN routing is evaluated in the presence of random-walk mobility without any specific locality information. The analyzed utility in those papers was computed by capturing short-term locality in nodes connectivity in the presence of node location information. In this paper, however, a key goal is to formulate modeling mechanisms that can capture multi-scale topological localities in human postural movements and use such locality information for modeling packet routing delay. In addition to general purpose DTN routing, including opportunistic [18–20], utility based [19–21], and random [19, 20], two other protocols, namely, PRMPL [23, 35], and DVRPLC [23, 35], which are specifically designed for on-body DTN routing, are also modeled in this paper.

3. Experimental Characterization of on-Body Network Topology

To model different routing protocols we have implemented a working WBAN prototype system. This section describes the *WBAN* prototype and its application for experimental topology characterization with varying body postural positions.

3.1. WBAN Prototype.
A *Wireless* Body Area Network (*WBAN*) is constructed by mounting seven sensor nodes (attached on two upper-arms, two thighs, two ankles, and one in the waist area) as shown in Figure 1. Each wearable node consists of a 900 MHz Mica2Dot MOTE (running TinyOS operating system), with Chipcon's SmartRF CC1000 radio chip (http://www.chipcon.com/), and the sensor card MTS510 from Crossbow Inc. (http://www.xbow.com/). The Mica2Dot nodes run from a 570 mAH button cell with a total sensor weight of approximately 10 grams. The default CSMA MAC protocol is used with a data rate of 19.2 kbps.

Via software adjustments of the CC1000's transmission power, the transmission range is set to be in between 0.3 m–0.6 m. By doing so, we are able to emulate the ultralow transmission range for the embedded transceivers [8–11] as reported in the literature. Note that the variation of the range is caused due to the variability in antenna orientation, clothing, and other on-body RF attenuation characteristics.

The sensors form a mesh topology with one or multiple simultaneous network partitions. The topology and the number of partitions change dynamically based on the postural positions of the subject individuals. All experiments in this paper correspond to multipoint-to-point routing in which data from all other nodes are sent to node-6 (see Figure 1), which is designated as the on-body sink node. This node collects raw data and sends processed results or events to an out-of-body server using a wireless link. This external
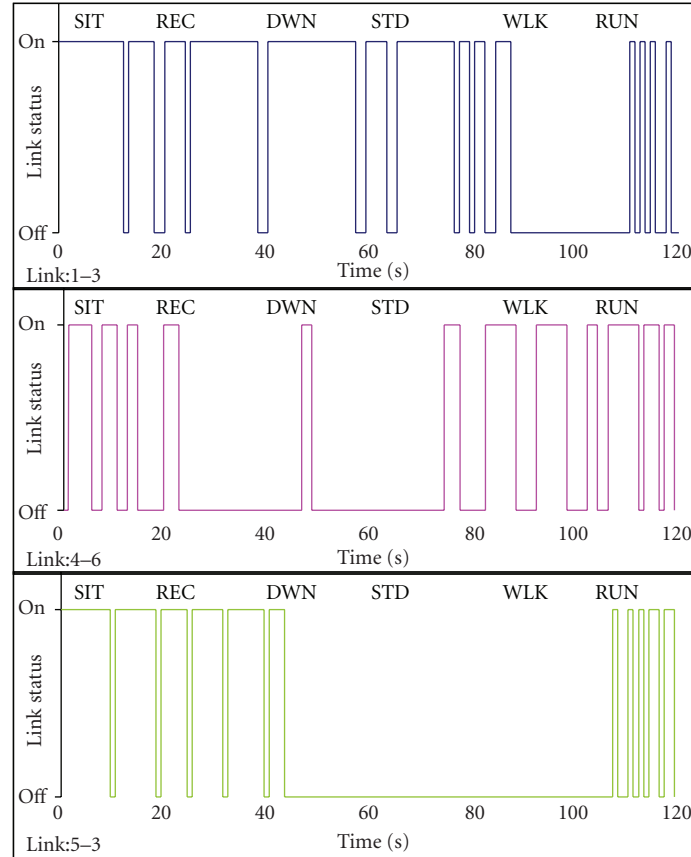
FIGURE 2: Variation of instantaneous link connectivity with postural mobility.

link is created between the on-body sink node and to an out-of-body Mica2Dot radio node connected to a Windows PC through a custom-built serial interface, running RS232 protocol.

3.2. Variations of Topology and Network Partitions. Experiments were carried out for observing the impacts of postural mobility on network partitioning. A human subject, fitted with seven sensors, was asked to follow a predetermined sequence of postures (SIT, SIT-RECLINING, LYING-DOWN, STAND, WALK, and RUN), each lasting for 20 sec. The status of three WBAN links (1–3, 4–6, and 5–3) during such an experiment is shown in Figure 2. The presence and absence of a link's connectivity, as sampled by the nodes on the link, is represented by 1 and 0, respectively.

Each node maintains a neighbor table based on *Hello* messages sent periodically with low transmission power once in 1.4 sec. A time-out period of 2.8 sec. is used for purging entries from the neighbor table. The link status in Figure 2 is constructed by combining the neighbor table information from the nodes relevant for the exhibited links. Experimentally, the neighbor table information is periodically sent by all seven on-body nodes to the out-of-body server (in Figure 1) using the full transmission power of the Chipcon's CC1000 radio.

The following observations can be made from Figure 2. First, few links are connected only during certain postures,

which can lead to significant topology variations and network partitioning across the postures. For instance, link 5–3 (between left front thigh and upper left arm nodes) shows the effect of distance on connectivity. The link is connected during most closed postures such as SIT and REC. However, for the stretched out postures such as LYING-DOWN, STAND, and WALK, the link is mostly disconnected. Similar trends are observed for the other links including link 1–3 and link 4–6, as shown in Figure 2.

The second observation is that even within a posture, a link may have intermittent disconnections (e.g., link 1–3 is disconnected during the SIT posture from "0–20" sec. interval). The reasons for such intraposture disconnections include minor body movements, RF signal blockage by body segments and clothing material, and also the relative orientations of the node-pairs forming the link in question.

The topology level impacts of the body posture variation are reported in Figure 3. Observe the wide swing of the node degree (1.5 to 3.8 across the six postures/activities) which indicates a high level of dynamism in the on-body mesh topology. Also observe the number of simultaneous network partitions which vary from 1 to 5, indicating frequent topological partitioning as hypothesized in Section 1.3. As expected, the postures with relatively lower node degree correspond to higher number of network partitions. Such topological disconnections necessitate on-body store-and-forward routing.
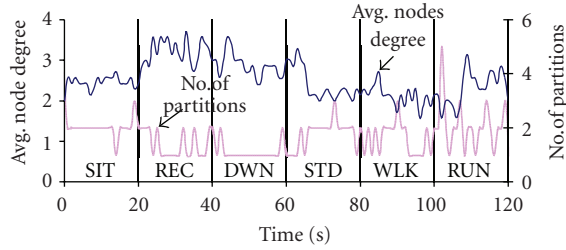
FIGURE 3: Instantaneous topology and partition properties with posture changes.

4. Topology Trace Collection for off-Body Routing Simulation

An objective of this paper is to develop delay models for different DTN routing protocols executed on dynamic *WBAN* topologies as depicted in Figure 3. A remote trace collection mechanism was developed so that real network topology traces from the prototype *WBAN* can be wirelessly collected and used for routing model development and off-line routing simulation experiments.

As depicted in Figure 4, during the on-body experiments, the state of each link (emulated using limited transmission power as shown in Figure 2) is periodically sent to the out-of-body server at full transmission power. The server collects the link-state samples (ON or OFF) from all the on-body links and stores them with a time-stamp from its local clock. All these link-state samples, together, form topology traces which are then used for delay model development and off-body routing simulations as presented in Sections 5, 6, and 8. Results from the delay model and off-body simulations are compared with the routing performance from the on-body experiments since all of them use the exact same topology traces, ensuring comparable link state and network partitioning patterns as discussed through the example in Figure 3.

5. Modeling DTN Routing Protocols

The objective of this section is to model the delay of (a) a series of existing single copy DTN routing algorithms applied to on-body settings and (b) two specific routing algorithms that are specifically developed to leverage the locality of *WBAN* topology as function of postural body movements.

Definition 1 (link state). The state of a link between two on-body nodes i and j at the nth discrete time slot is represented as $L_{i,j}(n)$, which is assigned the value 1 or 0 to indicate the state to be connected or disconnected, respectively. The time slot here is an observation time slot which corresponds to the *Hello* interval period for neighbor/link discovery. In our prototype implementation, it was set to be 1.4 sec.

Definition 2 (link disconnection probability). The Link Disconnection Probability (LDP) for the link between node-i and node-j is represented as $\hat{P}_{i,j}(k)$. The quantity $\hat{P}_{i,j}(k)$

represents the probability that after an arbitrarily chosen time slot, the link remains disconnected for k consecutive disconnected time slots. In a sufficiently long topology trace, spanning T time slots, if n_k represents the number of occurrences of such k-slot long disconnections, then the LDP can be expressed as

$$\hat{P}_{i,j}(k) = \begin{cases} \dfrac{n_k}{T}, & \text{for } k \geq 1, \\ \sum_{n=1}^{T} L_{i,j}(n)/T, & \text{for } k = 0. \end{cases} \quad (1)$$

The case $k \geq 1$ represents situations for which the arbitrarily chosen slot is a part of one of the T_{off} periods (except the last slot on the T_{off} period) or the last slot during one of the T_{on} periods (see Figure 5). Similarly, the case $k = 0$ represents situations for which the arbitrarily chosen slot is a part of one of the T_{on} periods (except the last slot on the T_{on} period) or the last slot during one of the T_{off} periods. With above definition of $\hat{P}_{i,j}(k)$, we have $\sum_{k=0}^{T} \hat{P}_{i,j}(k) = 1$, and its expected value can be represented as

$$ELD_{i,j} = \sum_{k=0}^{T} k \cdot \hat{P}_{i,j}(k), \quad (2)$$

where $ELD_{i,j}$ is the Expected Link Delay, representing the average number of disconnection slots after an arbitrarily chosen slot. In other words, $ELD_{i,j}$ can be expressed as $ELD_{i,j} = T_{\text{off}}^{i,j}/2$, where $T_{\text{off}}^{i,j}$ is the average disconnection duration for link i to j.

5.1. Opportunistic Routing.
In DTN opportunistic routing (OPPT) [18–20] a source node delivers packet to the destination node only when the two nodes come into direct contact. This single copy mechanism offers a simple DTN routing approach in which the delay can be very large, especially in scenarios with low mobility or infrequent link formation between the source and destination. This protocol is simple to implement and suited well for the processing- and energy-constrained on-body sensors for which complex algorithms should be avoided. It is highly energy efficient due to the single transmission requirement for each packet delivery. However, the expected packet delivery delay for OPPT can be quite high, especially when the source and the destination nodes are rarely in direct contact with each other. The protocol is also very sensitive to the source-destination link quality since it relies only on that single direct link for all packet delivery. Opportunistic routing is modeled and analyzed in this section for estimating the worst case delay performance and for finding an upper-bound for packet delivery delay in a *WBAN* setting.

Since a source node s delivers a packet to destination d only when $L_{s,d} = 1$ and a packet at node s can be generated at any arbitrary time slot, the delivery delay for a packet is $ELD_{s,d}$ as developed in (2). This is true only when the packet generation rate is low enough so that no more than one packet is generated during a T_{off} period (see Figure 5). This means that the generated packet can be delivered at the very beginning of the immediately following T_{on} period without any additional wait.
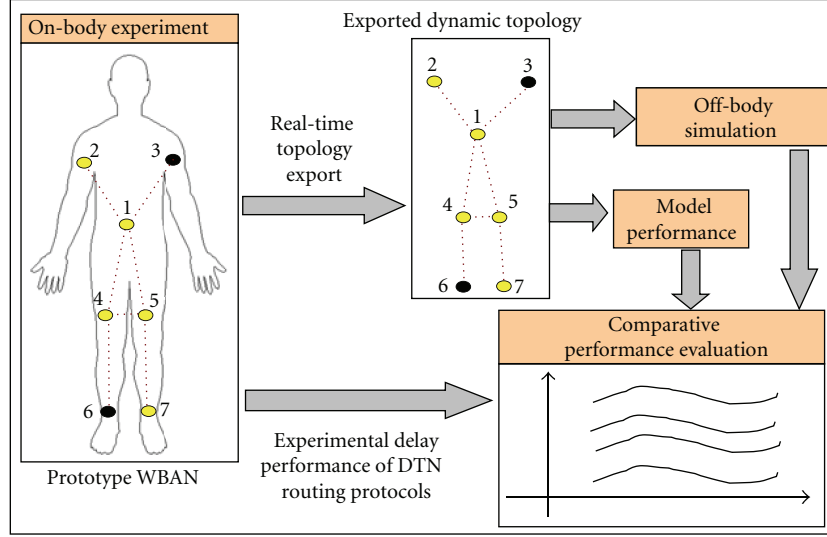
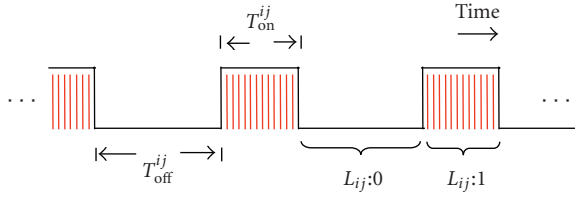FIGURE 4: Topology export for offline and model performance.

FIGURE 5: Example connectivity of an on-body link.

However, when the packet generation rate is higher so that multiple packets are generated during a T_{off} period, the packets need to be delivered one per time slot during the next T_{on} period. This backlog clearance adds an additional delay component that needs to be added in addition to the $ELD_{s,d}$ from (2). Let B represent the number of packets generated during the T_{off} period. With λ being the packet generation rate at the source node s, $B = \lambda \cdot T_{off}$. After the subsequent T_{on} period starts, these B packets are flushed one packet per time slot, requiring B time slots. During these B slots, another $B \cdot \lambda$ packets are generated which are then cleared one per slot.

Combining the backlog clearance delay with the Expected Link Delay (ELD), the average delivery delay for the packets generated during the T_{off} period can be written as $ELD_{sd} + \sum_{i=1}^{B-1} i/B$. Average delay for the packets generated during the T_{on} period can be written as $B/2 + \sum_{i=1}^{B\lambda-1} i$. Therefore, the overall average packet delay for on-body opportunistic routing can be expressed as

$$D_{\text{OPPT}} = \frac{(T_{off} \text{ Buffered Packets} \times T_{off} \text{ Avg} \cdot \text{Packet Delay}) + (T_{on} \text{ Buffered Packets} \times T_{on}\text{Avg} \cdot \text{Packet Delay})}{\text{Total Buffered Packets}} \quad (3)$$

or

$$D_{\text{OPPT}} = \frac{B \cdot \left(\text{ELD}_{sd} + \sum_{i=1}^{B-1} i\right) + B \cdot \lambda \cdot \left(B/2 + \sum_{i=1}^{B\lambda-1} i\right)}{B + B \cdot \lambda}, \quad (4)$$

where Expected Link Delay (ELD) can be computed in (2) and $B = \lambda \cdot T_{off}^{s,d} = 2 \cdot \lambda \cdot ELD_{s,d}$. Note that this expression is valid when the system is stable in the sense that on an average, all packets generated during the T_{on} and T_{off} periods are able to be delivered during the T_{on} period for the link between nodes s and d.

5.2. Randomized Routing. In randomized routing protocol (RAND), if a node with a data packet does not have a direct connection with the destination, the node forwards the data packet to a neighbor chosen at random [19, 20]. The packet is subsequently forwarded in the same way, till it is received at the destination. Unlike for hot-potato routing [20] in large networks, the delay performance of RAND can often be better than that of opportunistic routing in small body area networks only with few nodes. Smaller topologies have lesser number of end-to-end path combinations, leading to quicker delivery. Also, the network partitioning, as shown in Figure 3, helps reducing the path combinations even further. Packet looping, which is inherent in a randomized routing protocol, can be avoided by recording a packet's traversed path in it incrementally so that a forwarding filtering can be implemented. A packet is never forwarded to a node that is recorded in that packet's already traversed path. Like OPPT, the randomized protocol is also simple to implement but can deliver lower packet delay compared to OPPT. A packet being

$$A(1) = \begin{bmatrix} 0 & 0.5 & 0 & 0.5 \\ 1 & 0 & 0 & 0 \\ 0 & 0 & 0 & 0 \\ 0 & 0 & 1 & 0 \end{bmatrix}, \quad A(2) = \begin{bmatrix} 0 & 0 & 0 & 1 \\ 0 & 0 & 1 & 0 \\ 0 & 0 & 0 & 0 \\ 0.5 & 0.5 & 0 & 0 \end{bmatrix}, \quad A(3) = \begin{bmatrix} 0 & 0 & 1 & 0 \\ 0 & 0 & 1 & 0 \\ 0 & 0 & 0 & 0 \\ 0 & 0 & 1 & 0 \end{bmatrix}$$

$$[A(1) \cdot A(2)] = \begin{bmatrix} 0.25 & 0.25 & 0.5 & 0 \\ 0 & 0 & 0 & 1 \\ 0 & 0 & 0 & 0 \\ 0 & 0 & 0 & 0 \end{bmatrix}, \quad [A(1) \cdot A(2) \cdot A(3)] = \begin{bmatrix} 0 & 0 & 0.5 & 0 \\ 0 & 0 & 1 & 0 \\ 0 & 0 & 0 & 0 \\ 0 & 0 & 0 & 0 \end{bmatrix}$$
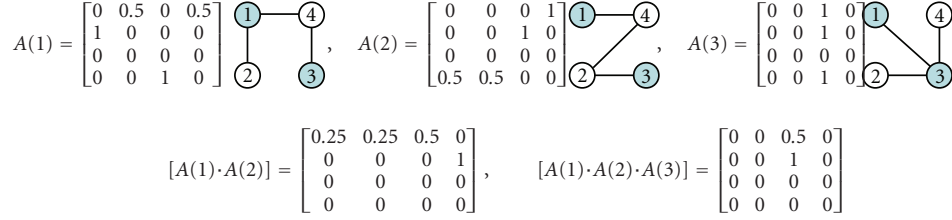
FIGURE 6: Example evolution of the forwarding matrix for a time-varying topology.

forwarded using the RAND protocol, however, can suffer from a large number of unnecessary forwarding before it is delivered at the destination. In other words, this protocol can be quite energy-inefficient.

Definition 3 (forwarding probability). In RAND forwarding, a node-i forwards a packet uniformly randomly to one of its currently connected neighbors. Therefore, at any time slot n, the probability of node i forwarding a packet to node j is defined as

$$P_{i,j}^f(n) = \frac{L_{i,j}(n)}{\sum_{j=1}^N L_{i,j}(n)}, \quad P_{i,i}^f(n) = 0, \quad \forall j \in N,$$

$$j \neq i, \ j \neq d, \quad \text{if } \sum_{j=1}^N L_{i,j}(n) \neq 0, \quad L_{i,d}(n) = 0, \tag{5}$$

where N is the number of nodes in the on-body network. Equation (5) is applicable as long as node i currently has at least one neighbor (i.e., $\sum_{j=1}^N L_{i,j}(n) \neq 0$), and none of those neighbors is the destination node d (i.e., $L_{i,d}(n) = 0$). In case when node i has destination d as a current neighbor, the packet is forwarded to node d with probability "1". Also, when node i has no current neighbors, it keeps buffering the packet (i.e., $P_{i,i}^f(n) = 1$), resulting in $P_{i,j}^f(n) = 0$, for all $j \neq i$. Incorporating all these situations, (5) can be expanded as

$$P_{i,j}^f(n) = \frac{L_{i,j}(n)}{\sum_{j=1}^N L_{i,j}(n)}, \quad P_{i,i}^f(n) = 0, \quad \forall j \in N,$$

$$j \neq i, \ j \neq d, \quad \text{if } \sum_{j=1}^N L_{i,j}(n) \neq 0, \quad L_{i,d}(n) = 0,$$

$$P_{i,d}^f(n) = 1, \quad P_{i,i}^f(n) = 0, \ P_{i,j}^f(n) = 0, \quad \forall j \in N,$$

$$j \neq i, \quad j \neq d \quad \text{if } L_{i,d}(n) = 1 \tag{6}$$

$$P_{i,i}^f(n) = 1, \quad P_{i,j}^f(n) = 0, \quad \forall j \in N,$$

$$j \neq i, \quad \text{if } \sum_{j=1}^N L_{i,j}(n) = 0.$$

Definition 4 (forwarding matrix). The forwarding matrix captures the forwarding probabilities at time slot n across all possible links in the network with N nodes and can be represented as

$A(n)$

$$= \begin{bmatrix} & 1 & 2 & \cdots & j & \cdots & N \\ 1: & P_{1,1}^f(n) & P_{1,2}^f(n) & \cdots & P_{1,j}^f(n) & \cdots & P_{1,N}^f(n) \\ 2: & P_{2,1}^f(n) & P_{2,2}^f(n) & \cdots & P_{2,j}^f(n) & \cdots & P_{2,N}^f(n) \\ \vdots & \vdots & \vdots & \cdots & \vdots & \cdots & \vdots \\ i: & P_{i,1}^f(n) & P_{i,2}^f(n) & \cdots & P_{i,j}^f(n) & \cdots & P_{i,N}^f(n) \\ \vdots & \vdots & \vdots & \cdots & \vdots & \cdots & \vdots \\ d: & 0 & 0 & \cdots & 0 & \cdots & 0 \\ \vdots & \vdots & \vdots & \cdots & \vdots & \cdots & \vdots \\ N: & P_{N,1}^f(n) & P_{N,2}^f(n) & \cdots & P_{N,j}^f(n) & \cdots & P_{N,N}^f(n) \end{bmatrix}. \tag{7}$$

The Forwarding Matrix $A(n)$ has two notable properties. First, the elements in the dth row are all zeros since the destination node d never forwards a packet. The elements in the dth column, however, are either 1 or zero (not explicitly shown above), depending on node d's instantaneous connectivity with the other nodes as expressed above in (6). Second, the summation of all elements in all rows (except the dth row) should be 1. The Forwarding Matrix, which depends on the link states $L_{i,j}(n)$, can be created after the forwarding probabilities are computed using (6) based on the observed link states from the collected WBAN topology traces.

Consider a data packet that is generated at node s during the nth time slot, and delivered to node d at the $(n+k)$th time slot, resulting in a delay of k slots. The value of k can vary from 0 to infinity. Let the probability of the above event (i.e., delivering the packet with a delay of k slots) be represented as the delivery probability $\rho_{s,d}^n(k)$, which can be expressed as

$$\rho_{s,d}^n(k) = [A(n) \cdot A(n+1) \cdot A(n+k)]_{s,d}$$

$$= \left[\prod_{i=0}^k A(n+i) \right]_{s,d} \tag{8}$$

which is the $[s, d]$ element of the product matrix for a packet generated at time slot $i = 0$ and delivered at time $i = k$. Equation (8) shows the probability of delivering a packet with a delay of k slots, where k can range from 0 to infinity.

Therefore, the expected RAND forwarding delay for a packet that was generated at the nth time slot can be written as

$$D_{\text{RAND}} = \sum_{k=0}^{T} k \cdot \rho_{s,d}^{n}(k) = \sum_{k=0}^{T} k \cdot \left[\prod_{i=0}^{k} A(n+i) \right]_{s,d}, \quad (9)$$

where T is the length (in number of slots) of the experimental topology traces obtained in Section 4. Considering sufficiently long on-body topology traces (i.e., large T), the maximum value of k in (9) is set to be T instead of infinity.

To clarify the above forwarding concept further, let us explore the following example in Figure 6. Consider a 4-node (i.e., $N = 4$) body sensor network with node-1 as the source and node-3 as the destination. Example forwarding matrixes $A(1)$, $A(2)$, and $A(3)$ and the corresponding network topologies at time slots 1, 2, and 3, obtained from the topology trace, are given in Figure 6.

Using the above matrixes, the delay probabilities can be computed as $\rho_{1,3}^{1}(0) = 0$, $\rho_{1,3}^{2}(1) = 0.5$, and $\rho_{1,3}^{3}(2) = 0.5$ using (8). According to $A(1)$, at time slot 1, node-1 has two neighbors (2 and 4), node-2 has one neighbor (node-1), and node-4 has a direct connection with the destination node-3. Assume that a packet is generated at source (node-1) at time slot 1. Since node-1 has no direct connection with d (i.e., $P_{1,3}^{f} = 0$), the packet will be randomly forwarded to either node 2 or 4 with probability 0.5 each, but the probability of delivering it to the destination node-3 is zero in the current slot-1 (out of all possible infinite number of slots in future). This is captured by $\rho_{1,3}^{1}(0) = 0$ which is the [1, 3] element of matrix $A(1)$.

At time slot 2, the packet will be forwarded to 3 through 2 with probability 1, that is, if 2 has already received the packet in slot 1. Otherwise (i.e., the packet was forwarded to node 4 in slot 1), the packet will be forwarded to node-1 or node-2 by node-4 at slot 2. Therefore, the probability of delivering the packet to the destination node-3 in slot-2 (out of all possible slots) is 0.5. This is captured by $\rho_{1,3}^{1}(1) = 0.5$ from the [1, 3] element of the product matrix $[A(1) \cdot A(2)]$.

Since $P_{1,3}^{f} = P_{2,3}^{f} = P_{4,3}^{f} = 1$ in $A(3)$, the packet is guaranteed to be delivered to node-3 in slot-3. Since the probability of delivery in slot-1 was zero, and in slot-2 was 0.5, and the delivery is guaranteed in slot-3 (i.e., if it was not delivered in slot-2), the probability of delivering the packet in slot-3 (out of all possible slots) is 0.5. In other words, the probability of delivery with a delay of 2 slots (i.e., $k = 2$) is 0.5. This is also captured as $\rho_{1,3}^{1}(2) = 0.5$ from the [1, 3] element of the product matrix $[A(1) \cdot A(2) \cdot A(3)]$. Using $\rho_{1,3}^{1}(0) = 0$, $\rho_{1,3}^{1}(1) = 0.5$, and $\rho_{1,3}^{1}(2) = 0.5$, the expected delay for random forwarding for this example WBAN topology trace is $0 \times 0 + 1 \times 0.5 + 2 \times 0.5 = 1.5$ time slots.

5.3. Utility-Based Routing Using Link Locality.
In randomized routing, a node does not consider the locality of its connectivity with other network nodes while forwarding a packet. In utility-based routing protocols [17–21], nodes prefer to forward packets to destination through the neighbor with the latest encounter with the destination, thus leveraging the link locality in the form of its age. Each node

is assigned a utility value based on the last encounter time with the destination, and a packet is forwarded to a neighbor with the highest utility value. Utility represents how useful (fast) this node might be in delivering a data packet to the destination and is often implemented using a timer. The delay of utility-based routing is expected to be lower than that in OPPT and RAND routing. Also, the number of packet forwarding in utility-based routing is expected to be smaller compared to RAND, mainly because of its exploitation of the link connection locality while selecting the next-hop during packet forwarding. The implementation of this protocol, however, can be more complex than OPPT and RAND because each node needs to compute and maintain the utility information for all neighbors in the network. Therefore, for large networks, maintaining utility information for every node can create significant scalability concerns. However, for small *WBAN*s this is less of an issue because of their small node-counts.

Let the utility function $U_{i,j}(n)$ represent the utility value, of node i with respect to node j at the nth time slot. Every time node i comes in contact with node j, the quantity $U_{i,j}(n)$ is set to a maximum utility value and then for every time slot the node remains out of contact from the destination, the quantity $U_{i,j}(n)$ is decreased based on a preset utility reduction method [19, 21] as a function of elapsed time. The update rule for $U_{i,j}(n)$ can be written as

$$U_{i,j}(n+1) = \begin{cases} U_{\max}, & \text{if } L_{i,j}(n+1) = 1, \\ U_{i,j}(n) - 1, & \text{if } L_{i,j}(n+1) = 0, \end{cases} \quad (10)$$

where $U_{\max}$ is the maximum possible utility value to the destination. These utility values are exchanged between neighbors within the periodic *Hello* messages.

With the above definition of utility, at the nth time slot node-i will forward a packet (destined to node-d) to node-j only if $U_{i,d}(n) < U_{j,d}(n)$ and $U_{j,d}(n) \geq U_{k,d}(n)$, forall $k \in \psi_i(n)$, where $\psi_i(n)$ is the set of all neighbors of node-i during the nth time slot.

Note that the above forwarding logic assumes that each on-body node is guaranteed to intermittently come within up to 2-hop contact from the destination node. In other words, a source node is able to meet other nodes that intermittently come in direct contact with the destination node. In our experimental topology this assumption was always found true [24]. In fact for a WBAN topology, it is generally true that depending on the specific postural patterns, all nodes intermittently form direct links with all other nodes in the network. This observation makes the assumption generally applicable for WBANs which usually have a small network diameter [19, 21]. When this 2-hop reachability assumption is not valid in large *WBANS*, transitive components will need to be incorporated while computing the utility factor.

The packet routing delay in utility-based forwarding (UTILITY) can be computed using the same logic as in random forwarding (RAND) except that the forwarding probabilities $P_{i,j}^{f}(n)$ in (6) need to be reformulated for

UTILITY. The forwarding probability in this case can be expressed as

$$P_{i,i}^{f}(n) = 1, \quad P_{i,j}^{f}(n) = 0,$$

$$\forall j \neq i \in N \text{ if } U_{i,d}(n) \geq U_{j,d}(n), \forall j \in \psi_i(n)$$

$$P_{i,j}^{f}(n) = 1, \quad P_{i,r}^{f}(n) = 0 \text{ if } U_{i,d}(n) < U_{j,d}(n), \quad (11)$$

$$U_{j,d}(n) \geq U_{k,d}(n), \quad \forall k \in \psi_i(n), \; \forall r \neq j \in N,$$

$$P_{i,d}^{f}(n) = 1, \quad P_{i,j}^{f}(n) = 0, \quad \forall j \neq d \in N \text{ if } d \in \psi_i(n),$$

where N represents the set of all on-body nodes and where $\psi_i(n)$ is the set of all neighbors of node-i during the nth time slot. The top line of (11) represents a situation in which either node-i does not have any neighbor during the nth time slot, or its own utility to the destination node-d is higher than those of all its current neighbors. Either way, the node buffers the packet with probability 1. The middle part of the equation codes the utility-based forwarding rule as stated after (11). The bottom part represents the situation in which the destination node-d is a direct neighbor of node-i, causing a direct delivery.

Once the forwarding probabilities are computed applying (11) on the on-body topology traces collected in Section 4, the forwarding matrix $A(n)$ and the delivery probabilities $\rho_{s,d}^{n}(k)$ are computed using the same rules presented in (7) and (8). Finally, the delivery delay is computed as $D_{\text{UTILITY}} = \sum_{k=0}^{T} k \cdot [\prod_{i=0}^{k} A(n+i)]_{s,d}$ using (9).

5.4. Probabilistic Routing with MultiScale Postural Locality (PRMPL). Routing using PRMPL utilizes a *Postural Link Cost* (PLC) [23] which captures WBAN link localities in multiple time scales. For on-body packet forwarding, the PLC is used exactly the same way as for the UTILITY routing, that is, by replacing the utility values by the PLCs. With posture and activity changes of a human subject, the PLC link costs are automatically adjusted such that the packets are forwarded to next-hops which are most likely to provide an end-to-end path with minimum intermediate buffering/storage delays. PLC is defined as $\beta_{i,j}(n)$, ($0 \leq \beta_{i,j}(n) \leq 1$), which represents the probability of finding $L_{i,j}(n) = 1$. The update equations for PLC are formulated as [23, 24, 36]

$$\beta_{i,j}(n) = \beta_{i,j}(n) + \left(1 - \beta_{i,j}(n-1)\right) \cdot \omega \quad \text{if link } L_{i,j}(n) = 1,$$

$$\beta_{i,j}(n) = \beta_{i,j}(n-1) \cdot \omega \quad \text{if link } L_{i,j}(n) = 0. \quad (12)$$

According to (12), when the link is connected, the *Postural Link Cost* (PLC) $\beta_{i,j}(n)$ increases at a rate determined by the constant $\omega (0 \leq \omega \leq 1)$, and the difference between the current value of $\beta_{i,j}(n)$ and its maximum value, which is 1. As a result, if the link remains connected for a long time, the quantity $\beta_{i,j}(n)$ asymptotically reaches its maximum value of 1. When the link is disconnected, $\beta_{i,j}(n)$ asymptotically reaches zero with a rate determined by the

constant ω. To summarize, for a given ω, $\beta_{i,j}(n)$ responds to the instantaneous connectivity condition of the link $L_{i,j}$.

With time invariant ω, the PLC update rules in (12) capture the locality in short-term link connectivity in a manner conceptually similar to the age-based utility formulation, as developed in [19, 21]. It is, however, not the same because in the designs in [19, 21], the routing utility of a link is increased incrementally when the link is formed and is reduced to zero as soon as the link is disconnected. This formulation of utility misses out the fact that even after disconnection, the formation probability of that link may be higher than a currently connected link. In other words, those definitions of utility fairly differentiate across currently connected links, but not across the currently nonconnected links. In the formulation of PLC in (12), motivated by the logic used in PROPHET [17], we track the short-term locality even when a link is not physically connected. This extended persistency in PLC is expected to improve performance over the existing age-based utility definitions as used in [19, 21].

The next design step is to dimension the parameter ω for capturing link localities at a longer time scale. From (12), the rate of change of the PLC $\beta_{i,j}(n)$ per time slot can be written as

$$\Delta\left(\beta_{i,j}(n)\right) = \left(1 - \beta_{i,j}(n-1)\right) \cdot \omega \quad \text{if link } L_{i,j}(n) = 1,$$

$$\Delta\left(\beta_{i,j}(n)\right) = -\beta_{i,j}(n-1) \cdot (1 - \omega) \quad \text{if link } L_{i,j}(n) = 0. \quad (13)$$

Equation (13) indicates that for a high ω (e.g., 0.9), $\beta_{i,j}(n)$ increases fast when the link is connected and decreases slowly when the link is not connected. Conversely, for a low ω (e.g., 0.1), $\beta_{i,j}(n)$ increases slowly when the link is connected and decreases fast when the link is not connected. Ideally, it is desirable that for a historically good link (i.e., connected frequently on a longer time scale), $\beta_{i,j}(n)$ should increase fast and decrease slowly, and for a historically bad link, it should increase slowly and decrease fast. This implies that the parameter ω needs to capture the long-term history of the link; hence it should be link specific and time varying. Based on this observation, we define *Historical Connectivity Quality* (HCQ) of an on-body link $L_{i,j}$ at time slot n as

$$\omega_{i,j}(n) = \frac{\sum_{r=n-T_{\text{window}}}^{n} L_{i,j}(r)}{T_{\text{window}}}. \quad (14)$$

The constant T_{window} represents a measurement window (in number of slots) over which the connectivity quality is averaged. The factor $\omega_{i,j}(n)$, ($0 \leq \omega_{i,j}(n) \leq 1$), indicates the historical link quality as a fraction of time the link was connected during the last T_{window} slots. The parameter T_{window} should be chosen based on the human postural mobility time constants. Experimentally, we found the optimal T_{window} values that work well for a large number of subject individuals and range of postures to be in between 7 sec. and 14 sec.

Figure 7 shows the evolution of PLC $\beta_{i,j}(n)$ and HCQ $\omega_{i,j}(n)$ with time. The top graph shows an example link activity (indicated by $L_{ij}(n)$) with the first half indicating a
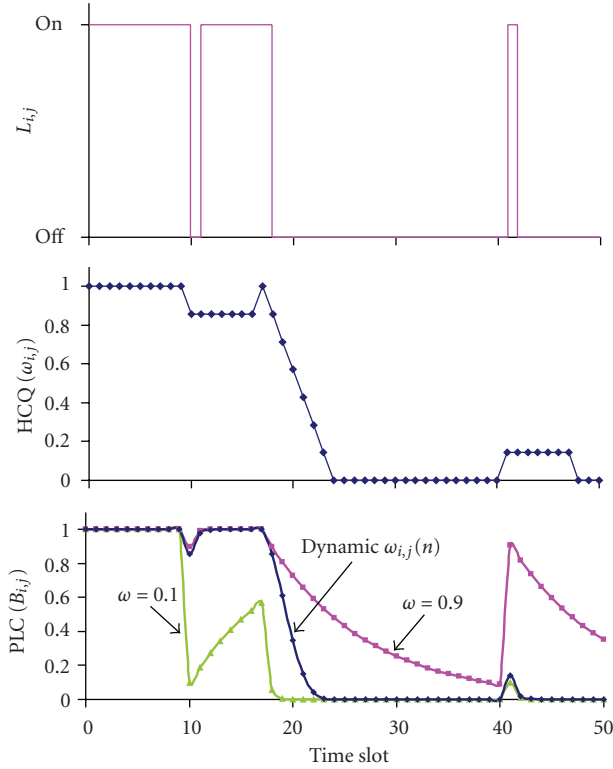
FIGURE 7: Evolution of multi-scale locality in terms of PLC and HCQ.

steadily connected link with a single time slot (1.4 sec.) of disconnection at time slot 10, and the second half indicates a steadily disconnected link with single slot of connection at the 41st slot. The top graph also shows the evolution of $\omega_{i,j}(n)$ according to (14) with a T_{window} set to 7 time slots. The bottom graph shows the evolution of $\beta_{i,j}(n)$ with constant ω (i.e., 0.9 and 0.1) and link-specific time varying $\omega_{i,j}(n)$ from (14), indicating the historical link quality. When the link is steadily well connected (during the first half), a high constant ω (i.e., 0.9) responds well to a momentary disconnection by decreasing $\beta_{i,j}(n)$ slowly, but recovering quickly when the link becomes reconnected. A low constant ω (i.e., 0.1) responds poorly in this situation by doing just the opposite, that is, a fast decrease and slow recovery.

Similarly, when the link is steadily disconnected (during the second half), a low constant ω (i.e., 0.1) responds relatively better than a high constant ω (i.e., 0.9) by increasing $\beta_{i,j}(n)$ slowly for a momentary connection, and decreasing $\beta_{i,j}(n)$ quickly after the link becomes disconnected. The lines for two constant ω values clearly show that a single constant value for ω is not able to handle both good-link and bad-link situations equally effectively.

As hypothesized, the link-specific and time-varying $\beta_{i,j}(n)$, on the other hand, is able to handle both situations well by mimicking the behavior of $\omega = 0.9$ during the historically good-link situation and that of $\omega = 0.1$ during the historically bad-link situation. These results clearly demonstrate the effectiveness of the HCQ and PLC concepts for designing routing utilities that can capture both short and

long-term localities of the on-body link dynamics. With this multi-scale approach, the proposed mechanism should be able to outperform both age-based (UTILITY) [19, 21] and probabilistic [17] routing protocols that use only short-term locality information.

Note that unlike the entities in Figures 2 and 3, the PLC and HCQ in Figure 7 show the link connectivity localities which depends on the short- and long-term history of the link. The localities captures in (12) and (14) are responsible for this memory-based behavior in Figure 7 in contrast to the instantaneous link behavior in Figures 2 and 3. Figure 8 summarizes the structural difference between PRMPL [36] and the UTILITY [19, 21] age-based protocol from the link locality capture standpoint. As shown in the figure, while UTILITY extracts only short-term locality from the link on-off dynamics, PRMPL extracts an additional long-term locality by observing the Historical Connectivity Quality (HCQ) as presented in (14). Additional complexity for PRMPL over OPPT, UTILITY, and RAND is expected due to its periodic computation of per-link HCQ and PLC.

The forwarding rule in PRMPL is identical to what stated for UTILITY-based forwarding in Section 5.3 with the utility function $U_{i,j}(n)$ replaced by the postural link cost $\beta_{i,j}(n)$. Consequently, the forwarding probabilities $P_{i,j}^{f}(n)$, the forwarding matrix $A(n)$, and the delivery probabilities $\rho_{s,d}^{n}(k)$ can be computed using (7), (8), and (11), respectively, and finally, the end-to-end packet delay can be computed as $D_{\text{PRMPL}} = \sum_{k=0}^{T} k \cdot [\prod_{i=0}^{k} A(n+i)]_{s,d}$ using (9).

5.5. Distance Vector Routing with Postural Link Costs (DVR-PLC).
In DVRPLC, nodes maintain end-to-end cumulative path cost estimates to a common sink node. Let us define a *Link Cost Factor* (LCF) $C_{i,j}(n)$, $0 \le C_{i,j}(n) \le C_{\max}$ which represents the routing cost for the link $L_{i,j}$ (between nodes i and j) during the discrete time slot n. The update equations for LCF are formulated as [23, 24, 36]

$$C_{i,j}(n) = C_{i,j}(n-1) \cdot \left(1 - \omega_{i,j}(n)\right) \quad \text{if link } L_{i,j}(n) = 1,$$

$$C_{i,j}(n) = C_{i,j}(n-1) + \left(C_{\max} - C_{i,j}(n-1)\right)$$
$$\cdot \left(1 - \omega_{i,j}(n)\right) \quad \text{if link } L_{i,j}(n) = 0.$$
$$(15)$$

When the link is connected, $C_{i,j}(n)$ decreases at a rate determined by $(1-\omega_{i,j}(n))$, where $\omega_{i,j}(n)$, $(0 \le \omega_{i,j}(n) \le 1)$ is the Historical Connectivity Quality, as defined in (14). If the link remains connected for a long time, the quantity $C_{i,j}(n)$ asymptotically reaches its minimum value 0. When the link remains disconnected, $C_{i,j}(n)$ increases at a rate determined by the quantity $(1 - \omega_{i,j}(n))$ and the difference between the current cost $C_{i,j}(n)$ and its maximum value 1. This formulation ensures that a link's routing cost always reflects the likelihood of the existence of the link while capturing its historical connectivity trends. Note that the time evolution of LCF in DVRPLC follows a rationale that is very similar to that of PLC in PRMPL. The main difference is that while the LCF reduces for connected links, the PLC increases in
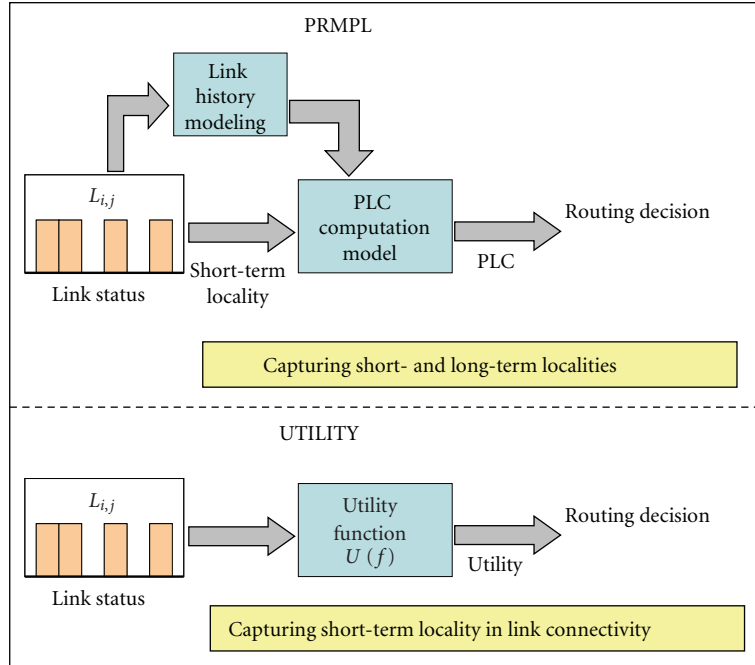
FIGURE 8: Capturing link connectivity locality in PRMPL and UTILITY age-based routing.

such situations. Similar difference exists when a link remains disconnected. To summarize, like in PRMPL, the cost in DVRPC captures both short- and long-term link localities for minimum delay packet routing.

Let $\gamma_{i,d}(n)$ be the minimum end-to-end cumulative cost from node-i to the sink node-d. According to distance vector routing logic, when a node i needs to forward a packet to the sink node d and it meets a node j, the packet is forwarded to node j only if the condition $\gamma_{j,d}(n) < \gamma_{i,d}(n)$ is found true. In other words, a lower path cost through node j indicates that the latter is more likely to forward the packet to node d than what node i's chances are. That justifies the packet transfer from node i to j with a goal of minimizing the end-to-end packet routing delay.

Note that the DVRPLC protocol attempts to minimize end-to-end cumulative routing costs. The objective is that due to this end-to-end cost minimization, DVRPLC should be able to outperform (from a delay standpoint) PRMPL which always interprets its PLC only at the link level and not in an end-to-end cumulative manner.

To execute DVRPLC, each on-body sensor node-i uses the periodic *Hello* mechanism, in order to gradually develop the $C_{i,j}(n)$ values with all other nodes in the network. It also iteratively updates the quantity $\gamma_{i,d}(n)$ using the computed $C_{i,j}(n)$ values with respect to all its neighbors. The node then uses the *Hello* mechanism to send the quantity $\gamma_{i,d}(n)$, its end-to-end cumulative path cost to the common destination *node-d* (e.g., node 6 in Figure 1), to all other nodes that are currently connected to *node-i*. This way, each node gets updated about the path costs of all of its direct neighbors' to the common destination *node-d*. The update equation for $\gamma_{i,d}(n)$

$$\gamma_{i,d}(n) = \min(\gamma_{i,d}(n),\ \gamma_{k,d}(n) + C_{i,k}(n)), \qquad (16)$$

where node-k has the minimum $\gamma_{k,d}(n)$ among all the current neighbors of node-i.

Because of its end-to-end nature, the forwarding rule in DVRPLC is based on the end-to-end cost $\gamma_{i,d}(n)$ as opposed to that based on local parameters $U_{i,j}(n)$ or $\beta_{i,j}(n)$ as used in UTILITY and PRMPL both of which do not rely on end-to-end cost. The distance vector forwarding rule for a packet from node-i to destination node-d can be formalized as follows. If node-i is a direct neighbor of node-d, forward the packet. Otherwise find node-k such that node-k has the minimum $\gamma_{k,d}(n)$ among all the current neighbors of node-i. Then forward the packet to node-k only if $\gamma_{k,d}(n) < \gamma_{i,d}(n)$; otherwise, continue buffering the node as node-i. With this forwarding rule, the forwarding probabilities $P_{i,j}^f(n)$ can be expressed as

$$P_{i,d}^f(n) = 1,\ P_{i,j}^f(n) = 0, \quad \forall j \neq i, d \in N \text{ if } L_{i,d}(n) = 1,$$

$$P_{i,k}^f(n) = 1,\ P_{i,j}^f(n) = 0, \quad \forall j \neq i, k \in N \text{ if } L_{i,d}(n) \neq 1,$$

$$\begin{matrix} \gamma_{k,d}(n) < \gamma_{i,d}(n), \\ \gamma_{k,d}(n) \leq \gamma_{r,d}, \end{matrix} \quad \forall r \in \psi_i(n), r \neq i,\ d, k \in N,$$

$$P_{i,i}^f(n) = 1,\ P_{i,j}^f(n) = 0, \quad \forall j \neq d, i \in N \text{ if } L_{i,d}(n) \neq 1,$$

$$\begin{matrix} \gamma_{k,d}(n) \geq \gamma_{i,d}(n), \\ \gamma_{k,d}(n) \leq \gamma_{r,d}, \end{matrix} \quad \forall r \in \psi_i(n), r \neq i,\ d, k \in N,$$

$$(17)$$

where N represents the set of all on-body nodes and where $\psi_i(n)$ is the set of all neighbors of node-i during the nth

time slot. The forwarding matrix $A(n)$ and the delivery probabilities $\rho_{s,d}^n(k)$ can be computed using (7) and (8), respectively, and finally, the end-to-end packet delay can be computed as $D_{\text{DVRPLC}} = \sum_{k=0}^{T} k \cdot [\prod_{i=0}^{k} A(n+i)]_{s,d}$ using (9).

6. Routing Delay Benchmark

In order to determine the best case end-to-end delay performance, an offline route search algorithm, *Backward Search for Delay Benchmark Routing (BSDBR)*, has been developed. As long as the entire topological sequences for a dynamically partitioned network are known a priori, the BSDBR algorithm is able to compute the most delay optimal end-to-end path for each packet depending on its source, destination, time of origin, and the complete topological sequence information. BSDBR is designed to be an offline centralized search algorithm, to be executed in the presence of entire time series topology information.

Let t^0 be the time instant at which a packet is generated at node-i and routed towards destination node-d. Given a known topology sequence, the objective is to find the earliest time instant after t^0 at which the packet can be delivered to the destination. Let t^1 be the earliest time instant ($t^1 > t^0$) at which destination node-d comes in contact with any other node-j ($j \in N$, $j \neq d$). The minimum possible delivery delay for the packet originated at time t^0 can be written as ($t^1 - t^0$). This minimum delay is possible only if the necessary network links are formed across the network during the time interval [t^0 to t^1] so that the packet could be forwarded multihop all the way from the origin node-i to node-j before time t^1. The objective of *BSDBR* search process is to scan the network topology sequence in order to find if such link formations are there so that ($t^1 - t^0$) can represent the minimum packet delivery delay.

If the search process concludes that the packet cannot be delivered by time t^1, then the next feasible time instant t^2 is identified, and a similar search is conducted to determine if ($t^2 - t^0$) can be the minimum delivery delay. The quantity t^2 is the earliest time instant after t^1 ($t^2 > t^1$) at which destination node-d comes in contact with any other node-j ($j \in N$, $j \neq d$). This BSDBR search process is iteratively continued till a valid minimum delivery delay ($t^r - t^0$) is found. The time instant t^r corresponds to the earliest contact time so that the necessary network links are formed across the network during the time interval [t^0 to t^r] so that the packet can be forwarded multi-hop all the way from the origin node-i to destination node-j by the time t^r.

Note that the expected value of the packet delay lower bound could have been computed using the Linear Programming formulation as adopted in the full knowledge-based approach in [28]. Instead, we have chosen to implement BSDBR since it allows us to determine the minimum packet delay for each individual packet as opposed to their average in a statistical sense. Also, the formulation in [28] is more complex than BSDBR since it incorporates the effects of message queuing which is not studied in our implementation.

7. Performance Evaluation

The same seven-sensor laboratory prototype network, as shown in Figure 1, was used for the on-body experimental evaluation of all the analyzed routing protocols. Packets originated from all sensors were routed to the common destination node-6, attached on the right ankle. Unless stated otherwise, results correspond to packets originated from node-3, representing the longest hop (i.e., also worst case) packet routing scenario in most of the body postures. Results are also presented from off-body simulation experiments, carried out on network topology traces collected during the actual on-body experiments so that the simulation results can be compared with the experimental data for the exact same topology traces. Those traces are also used to create the forwarding matrix in (7) for computing the analytical packet delay numbers for all the analyzed routing protocols.

In order to avoid the CSMA MAC collisions inherent to Mic2Dot's TinyOS networking stack, we have implemented a higher-layer polling access strategy managed by one on-body node. This polling node polls the other six-sensor nodes in a round-robin fashion, so that a regular node forwards packets (both data and Hello) only when it is polled by the polling node and given access to the channel. A polling time frame of 1.4 sec. is used which is divided into 7 time slots, one for each of the seven on-body nodes. Note that the polling node itself also needs to send Hello packets and so forth, for link cost formulation as described in Section 3. Although the data packets and the Hello messages from the nodes are transmitted at software power-adjusted transmission range of 0.3 m–0.6 m, the polling packets are transmitted by the polling node at full power so that all on-body nodes receive such packets. If a node misses a polling packet in a frame due to channel error, it misses transmission opportunity only in that frame.

7.1. Performance Metrics. The primary performance index is the end-to-end *Packet Delay* (PD), which is modeled in this paper and is attempted to be explicitly minimized by the UTILITY, PRMPL, and DVRPLC protocols as presented in Sections 5.3, 5.4, and 5.5. Unlike in conventional unpartitioned networks, the PD in partitioned on-body networks depends mainly on the storage delay at the intermediate nodes. Two secondary metrics, namely, *Packet Hop Count* (PHC) and *Packet Delivery Ratio* (PDR), are also recorded for a more complete understanding. The index PHC captures the number of forwarding per packet delivery, indicating the transmission energy expenditure; it does not indicate the packet delay since the PD in this context depends more on the buffering/storage than on the hop-count.

7.2. Traffic Generation and Data Collection. A chosen source node is programmed to generate data packets at the rate of 1 packet every 4 discrete time slots (each slot is 1.4 sec), with a packet size of 46 bytes. All on-body network nodes are slot-level time-synchronized by the sink node (i.e., node-6 in Figure 1) using periodic synchronization packet broadcast at a high transmission power [23]. By stamping a packet with the transmission time slot-id by the source node and
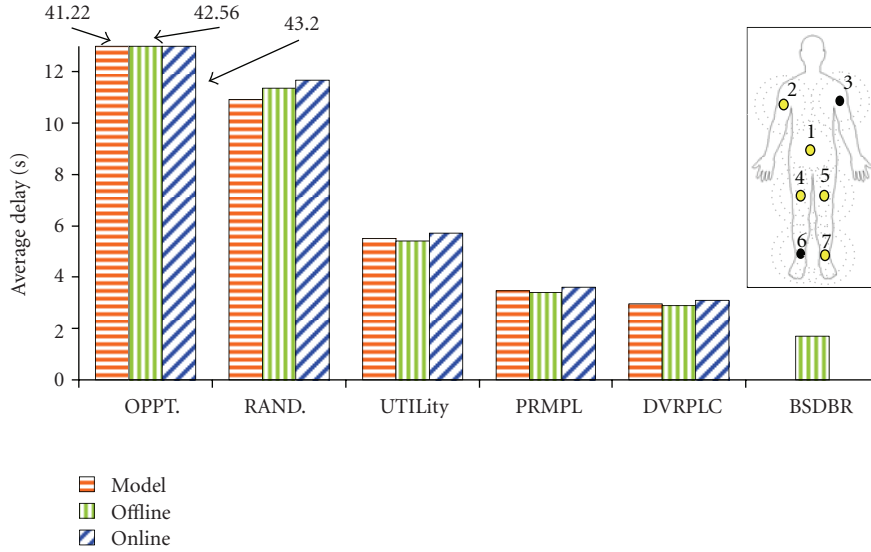
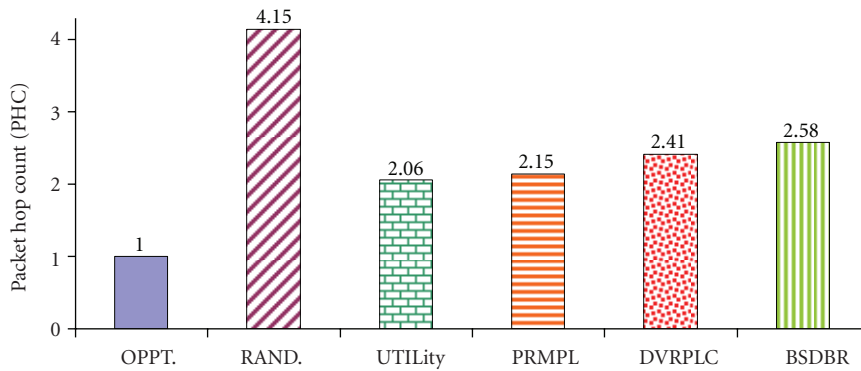FIGURE 9: On-body packet delivery delay for different DTN routing protocols.

FIGURE 10: Average packet hop count.

subtracting it from the reception time slot-id at the sink node, it is possible to compute the single-trip packet delay (PD) at the sink node. On its way to the sink node, a data packet collects the entire route information in the form of a list of the intermediate node-IDs. This allows the extraction and analysis of route information including the PHC values.

7.3. Packet Delay (PD). End-to-end packet delivery delays for a packet from the source node-3 on left upper arm to the sink node-6 on right ankle for all routing protocols analyzed in Section 5 are reported in Figure 9. For each of these protocols, a separate experiment was run for 1320 sec. (i.e., 22 minutes), sending 230 packets, and spanning 6 different body postures and activities (SIT, SIT-RECLINING, LYING-DOWN, STAND, WALK, and RUN), each lasting for 20 sec. Figure 9 reports the average of packet delay computed from the analytical model, on-body experiment, and off-body simulation using network topology traces collected during the on-body experiments. The figure also shows the delay lower-bound obtained by applying the BSDBR benchmark

algorithm (presented in Section 6) on the topology traces collected from on-body experiments.

The following observations can be made in Figure 9. First, the experimental, simulation, and model-generated analytical results closely match across all protocols. Second, as a general trend the delay performance improves with the amount of knowledge leveraged on topological locality. Both PRMPL and DVRPLC achieve significantly better delay compared to the other protocols and very close to BSDBR benchmark delay, because they are able to capture multi-scale topological localities in human postural movements using the cost parameters $\beta_{i,j}(n)$ and $C_{i,j}(n)$, as explained in Sections 5.4 and 5.5. The age-based approach UTILITY uses only the short-term locality, which explains its larger delay compared to PRMPL and DVRPLC, but smaller delay than OPPT and RAND, both of which do not leverage any topological locality information and responds based solely on instantaneous link conditions. Randomized forwarding provides slightly better delay since in a typically small WBAN, there are only few possible end-to-end path combinations, leading to quicker delivery than the opportunistic
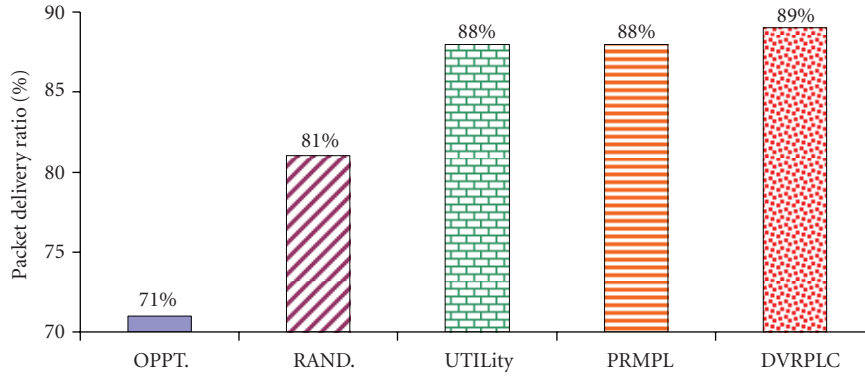
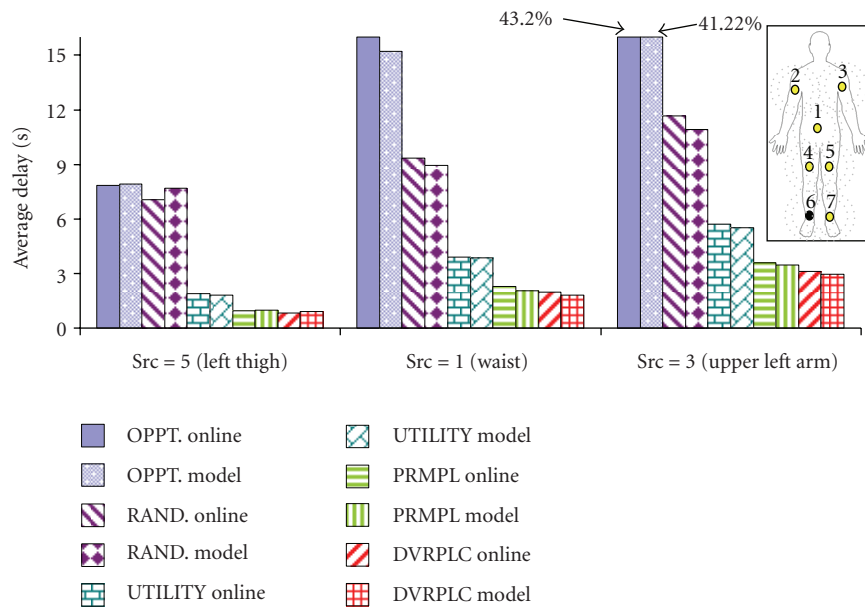FIGURE 11: Packet delivery performance observed for different protocols.

FIGURE 12: Delivery delay for packets from thigh, waist, and arm to right ankle (i.e., node 6).

mode in which a delivery is possible only when the source directly meets the destination.

7.4. Packet Hop Count (PHC). Figure 10 shows the average PHC which serves as an indirect measure for communication energy expenditure (i.e., for transmission and reception) for the on-body sensors. The large number for RAND explains the impacts of random forwarding compared to all other protocols. The protocols DVRPLC and BSDBR take slightly longer routes compared to the other protocols, although those two offer better packet delays. This means that they route packets through better quality links, leading to smaller delays, even though it requires more number of end-to-end hops. Since the opportunistic routing (OPPT) packets are delivered only when a source comes in direct contact of the destination, all packets are delivered with PHC 1.

7.5. Packet Delivery Ratio. Since no link layer packet retransmissions are deployed, the system is not able to recover from the packet drops observed due to the following reason. Due to postural mobility, there are transient blackout periods during which a neighbor may appear to be connected in a node's neighbor table, when in fact it is no longer connected. These blackout periods are created during a node's neighbor time-out period, which was chosen to be two polling frames or 2.8 sec, as reported in Section 3.2. Packet transmissions during such blackout periods end up in packet drops since no link layer reliability is used. All five evaluated protocols suffer from such packet losses, which are captured in the Packet Delivery Ratio (PDR) as reported below.

In Figure 11, the poor PDR for the OPPT protocol is caused due to a very unreliable link between the source and the destination nodes (i.e., nodes 3 and 6 in Figure 1) which

are physically situated at two extremes of the subject's body. Since the OPPT protocol relies on direct source-destination contact for packet delivery, the source-destination link quality affects this protocol most. For RAND, since the hop count is large (see Figure 10), it is more likely for a packet to encounter the transient blackout period during its end-to-end trajectory, thus leading to higher drops and low PDs. Lower hop-counts (see Figure 10) for the locality-based protocols, namely, UTILITY, PRPML, and DVRPLC, suffer from fewer drops due to the relatively lower occurrences of the transient blackouts. Note that the concept of such drops do not apply for the Benchmark case and that is why there is no entry for BSDBR in Figure 11.

7.6. Routing Packets from and to Different Body Segments. Delivery delays computed using the developed model and from on-body experiment for packets from different body segments to the sink node placed on the right ankle (i.e., node 6 in Figure 1) are shown in Figure 12. As shown in the figure, the experimental and model-generated analytical results closely match across all protocols. Observe that as the physical distance between a source and the destination increases, the average packet delivery delays for all the protocols increase. Relatively though, all the experimented routing protocols maintain the same trend for the packet delay as observed in Section 7.2 The average packet hop-counts from source nodes 5, 1, and 3 were experimentally logged in the range of 1.25, 1.5, and 2.3, respectively.

Similar trends in the delivery delay were experimentally observed for a large number of other combinations of source and destination nodes placed at different body segments. Although the absolute delay values were different, the overall trend in packet delay follows the same pattern for all such combinations that were experimented with.

7.7. Impacts of Postural Stability. For all the experiments so far, each individual physical posture was made to last for 20 sec. In order to study the impacts of variable postural stability on the routing performance, the subject was instructed to repeat the same sequence of postures as in Section 3, but with different posture durations ranging from 10 sec. to 40 sec.

Figure 13 shows the impacts of posture duration on average packet delay for all five protocols. Due to its significantly higher values, the packet delays for the OPPT protocol are plotted as a separate axis in Figure 13. Observe that the packet delays for all the protocols generally increase with higher posture durations. This is because longer posture duration implies that a connected link remains connected for longer duration and also a disconnected link remains disconnected longer. As a result, a packet that is buffered in a node due to network partitioning remains buffered for longer duration, leading to higher end-to-end delay. In a relative sense, all the experimented protocols maintain the same performance trend for packet delay as observed in Section 3, Figure 9. It should be observed that the packet delays for the protocols UTILITY, PRPML, and DVRPLC maintain very similar difference for a wide range of the posture duration mainly because of the fact that all three of
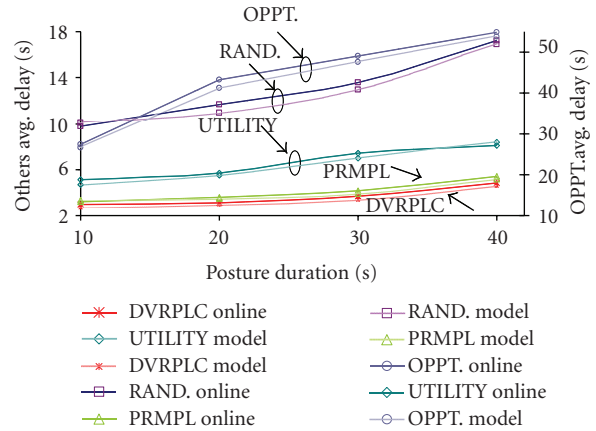

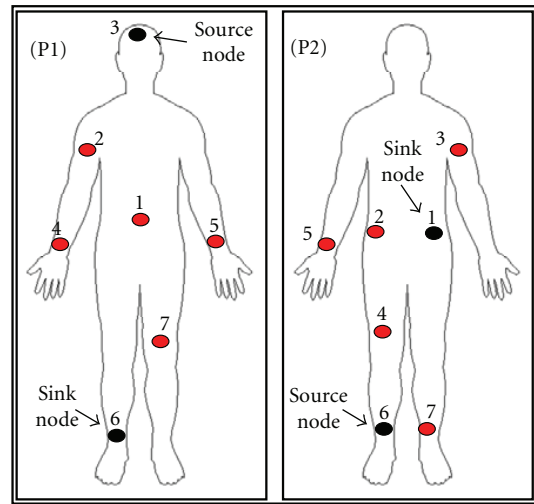Figure 13: Impacts of posture duration on packet delay.

Figure 14: Experiments with different sensor placements.

them use the link locality information, leading to the similar trend of variation with posture duration.

7.8. Impacts of Sensor Placements. Additional on-body sensor placements, as shown in Figure 14, were experimented with for evaluating the validity of the routing results obtained so far from the sensor placement shown in Figure 1. Different source and sink nodes are used in the two placement settings P1 and P2 in Figure 14. The inter-posture sequence, described in Section 3.2, was followed by a subject and the corresponding packet delay results are presented in Figure 15 for the placement settings P1 and P2 in Figure 14. Generally, the relative performance trends across all the experimented protocols as observed for the original sensor placement (in Figure 9) remain valid for the new sensor placements P1 and P2 in Figure 14. The delay for placement P1 is larger due to the longer source-to-destination distance compared to that in P2.

Note that the impacts of link failure were not separately studied because the effects of such failures have already been
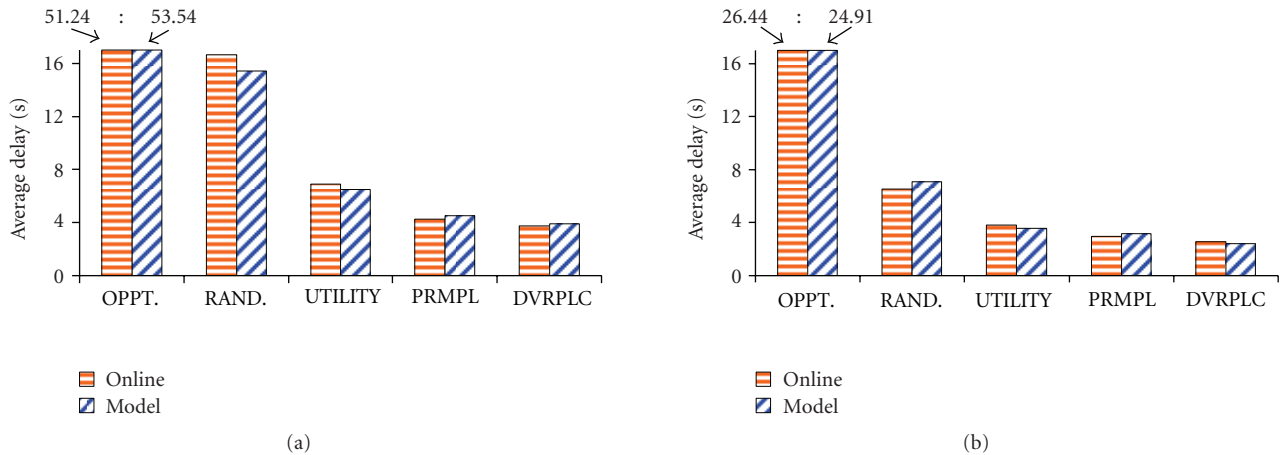
FIGURE 15: On-body packet delay for (a) sensor placement P1 and (b) sensor placement P2.

captured via link disconnection in a DTN network. Also, for a given node placement (e.g., Figures 1 and 14), the dynamic postures (e.g., walk and run) and the variability in the posture duration create sufficient amount of dynamism and diversity in the network topologies, leading to a generalized validation of the presented approach.

8. Evaluation of Node Criticality

The objective of this section is to evaluate the topological criticality of the WBAN sensor nodes. Once identified, such criticality information can be used for selectively reducing the on-body sensor-count without substantially sacrificing the packet delivery delay. The mechanism for such analysis is to first remove all links attached to a certain number of sensor nodes from the collected topology trace (see Section 4) and then run off-line routing simulation experiments to evaluate the new delay on this reduced network. Comparison between the delays from the original trace and this reduced trace would indicate the topological criticality of the removed node combination from a routing standpoint.

The above mechanism is applied to the 7-node WBAN with node-3 as the source and node-6 as the destination as shown in Figure 1. Figure 16 shows the resulting end-to-end packet delay characteristics when a single node (chosen from the set 1, 2, 4, 5, or 7) is selectively removed from the network under different routing protocols. Figure 16(a) shows the new delay after a node is removed, and Figure 16(b) shows the difference between the new delay and delay obtained from the complete topology without any node removed. The latter indicates the topological criticality of the removed node from a routing standpoint. A positive low difference in Figure 16(b) would indicate that the removed node is not particularly critical for the corresponding routing protocol. Conversely, a positive high difference would indicate that the removed node is critical. A negative difference actually means that the routing performance has improved after the node is removed. This means that the corresponding routing protocol was nonoptimally choosing the node after

removing which the routing protocol actually found a better route, leading to lower delay. Results for all the analyzed protocols except opportunistic routing (OPPT) are presented in Figure 16. Since OPPT relies on direct source-destination contact for packet delivery, removal of any intermediate node from the topology does not impact the delivery delay, which is why it is not included.

Observe in Figure 16(b) that removing a node from the network creates different amount of delay difference depending on the specific routing protocol. Note that for the age-based UTILITY routing the delay difference is negative, although small, when any of the nodes 1 or 2 is removed. This indicates that UTILITY was non-optimally choosing those two nodes and by removing any of them is forcing the protocol to choose a better route, resulting in negative difference. This inaccuracy is introduced by the short-term-only connectivity locality in the protocol. On the other hand, by leveraging both short- and long-term connectivity locality, as introduced in Sections 5.4 and 5.5, the protocols PRMPL and DVRPLC completely eliminate the negative differences, which means that they always choose an optimal route through nodes removing which actually worsens the delay. Similarly, in Figure 16(b), the BSDBR algorithm with benchmark delay also demonstrates optimal routes indicated by no negative differences. Finally, observe that the node dependencies of the RAND are generally more than those of all other protocols mainly because with randomized forwarding any node in WBAN can be in a packet's path as described in Section 5.2. In other words, since there are no constrains on packet forwarding with the RAND protocol, removing any node from the set 1, 2, 4, 5, or 7 can significantly impact the end-to-end packet delivery delay.

From the results in Figure 16(b), the following conclusions can be made. First, if PRMPL or DVRPLC (these two provide the best end-to-end delay as shown in Figure 9) is deployed, one node from the set 1, 2, and 7 can be easily removed without sacrificing packet delay. Second, generally, nodes 4 and 5 are topologically more critical than all other nodes (in the context of source 3 and destination 6) primary
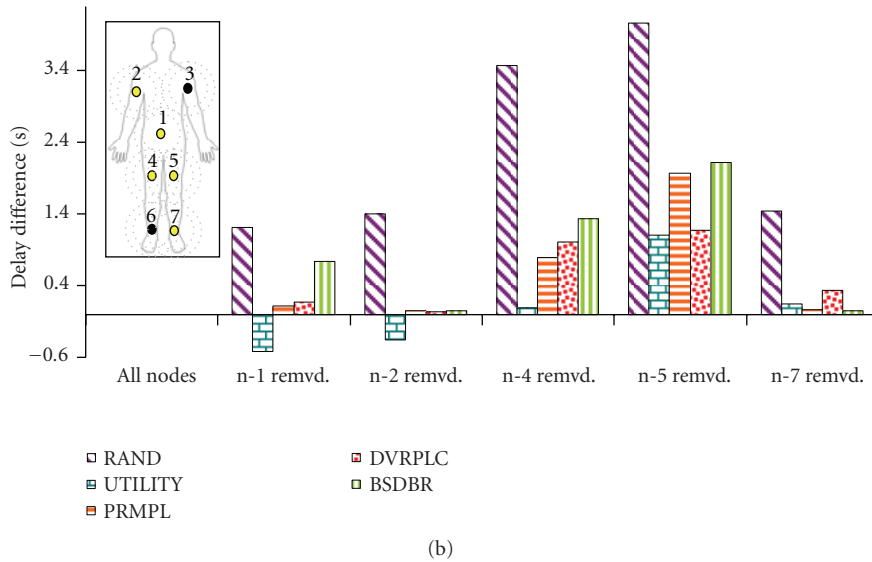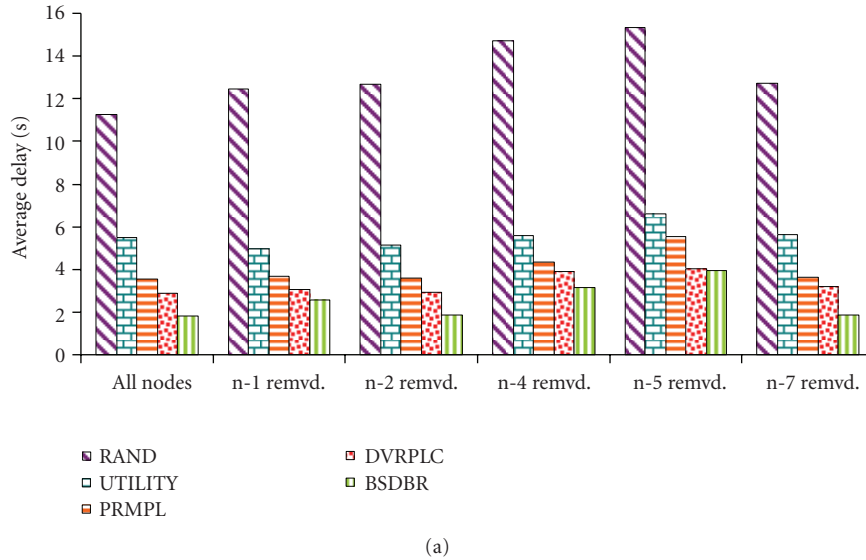
(a)

(b)

FIGURE 16: Single node criticality in terms of (a) packet delay and (b) packet delay difference.

because of their physical proximity to the destination and physical placement with respect to possible routes from node-3 to node-6.

Note that the analysis in this section shows what happens if only one node is removed from the topology. In order to find the impacts of removing multiple nodes, similar analysis can be done by removing different combinations of the nodes and then by measuring the delay differences. Also, removal of a node will be feasible only if the primary purpose of the node is routing and not sensing.

9. Conclusion and Ongoing Work

This paper develops a delay modeling framework for store-and-forward packet routing in Wireless Body Area Networks (*WBANs*). Using a prototype *WBAN* for experimentally

characterizing and capturing on-body topology traces, an analytical delay modeling technique was developed for evaluating single-copy DTN routing protocols. End-to-end routing delays for a series of protocols including opportunistic, randomized, and two other mechanisms that capture multi-scale topological localities in human postural movements have been evaluated. Performance was evaluated experimentally, via simulation, and using the developed models. It was shown that via multi-scale modeling of the spatiotemporal locality of on-body link disconnection patterns, it is possible to attain better delay performance compared to opportunistic, randomized, and utility-based DTN routing protocols in the literature. Finally, a mechanism for evaluating the topological importance of individual on-body sensor nodes is developed. It is shown that such information can be used for selectively reducing the on-body sensor-count without

substantially sacrificing the packet delivery delay. Ongoing work on this topic includes developing a Kalman Filter based body movement prediction model for predictive on-body packet routing with lower delay objectives.

Acknowledgments

References

[1] E. Jovanov, A. Milenkovic, C. Otto, and P. C. De Groen, "A wireless body area network of intelligent motion sensors for computer assisted physical rehabilitation," *Journal of NeuroEngineering and Rehabilitation*, vol. 2, article 6, 2005.

[2] M. Quwaider and S. Biswas, "Body posture identification using hidden Markov model with a wearable sensor network," in *Proceedings of the ICST 3rd International Conference on Body Area Networks*, Tempe, Ariz, USA, 2008.

[3] "WebPage of Department of Health and Human Services," http://grants2.nih.gov/grants/guide/pa-files/PA-07-354.html.

[4] K. Y. Chen and D. R. Bassett Jr., "The technology of accelerometry-based activity monitors: current and future," *Medicine and Science in Sports and Exercise*, vol. 37, no. 11, pp. S490–S500, 2005.

[5] M. Quwaider and S. Biswas, "Physical context detection using multi-modal sensing using wearable wireless networks," *Journal of Communication Software and Systems*, vol. 4, pp. 191–202, 2008.

[6] S. Lin, J. Zhang, G. Zhou, L. Gu, J. A. Stankovic, and T. He, "ATPC: adaptive transmission power control for wireless sensor networks," in *Proceedings of the 4th International Conference on Embedded Networked Sensor Systems (SenSys '06)*, pp. 223–236, ACM Press, November 2006.

[7] S. Xiao, V. Sivaraman, and A. Burdett, "Adapting radio transmit power in wireless body area sensor networks," in *Proceedings of the ICST 3rd International Conference on Body Area Networks*, Tempe, Ariz, USA, 2008.

[8] S. Mikami, T. Matsuno, M. Miyama, M. Yoshimoto, and H. Ono, "A wireless-interface SoC powered by energy harvesting for short-range data communication," in *Proceedings of the 1st IEEE Asian Solid-State Circuits Conference (ASSCC '05)*, pp. 241–244, November 2005.

[9] D. Sagan, *Integrated Circuits for Medical Applications: Meeting the Challenge of Ultra Low Power Communication*, Ultra-Low-Power Communications Division, Zarlink Semiconductor, 2005.

[10] E. Strömmer, M. Hillukkala, and A. Ylisaukkoja, "Ultra-low Power Sensors with Near Field Communication for Mobile Applications," in *Proceedings of the International Conference on Wireless Network (ICWN '07)*, 2007.

[11] T. Falck, H. Baldus, J. Espina, and K. Klabunde, "Plug 'n play simplicity for wireless medical body sensors," in *Proceedings of the Pervasive Health Conference and Workshops (Pervasive-Health '06)*, December 2006.

[12] E. Jones and P. Ward, "Routing strategies for delay-tolerant networks," in *Proceedings of the 2006 International Conference on Wireless Communications and Mobile Computing*, Vancouver, Canada, 2006.

[13] H. Guo, J. Li, Y. Qian, and Y. Tian, "A practical routing strategy in delay tolerant networks using multiple pigeons,"

in *Proceedings of IEEE Military Communications Conference (MILCOM '08)*, November 2008.

[14] J. Leguay, T. Friedman, and V. Conan, "Evaluating Moby-Space-based routing strategies in delay-tolerant networks," *Wireless Communications and Mobile Computing*, vol. 7, no. 10, pp. 1171–1182, 2007.

[15] V. Conan, J. Leguay, and T. Friedman, "Fixed point opportunistic routing in delay tolerant networks," *IEEE Journal on Selected Areas in Communications*, vol. 26, no. 5, Article ID 4530734, pp. 773–782, 2008.

[16] J. Leguay, T. Friedman, and V. Conan, "Evaluating mobility pattern space routing for DTNs," in *Proceedings of the 25th IEEE International Conference on Computer Communications (INFOCOM '06)*, April 2006.

[17] A. Lindgren, A. Doria, and O. Schelén, "Probabilistic routing in intermittently connected networks," *ACM SIGMOBILE Mobile Computing and Communications Review*, vol. 7, no. 3, pp. 19–20, 2003.

[18] T. Spyropoulos, K. Psounis, and C. S. Raghavendra, "Efficient routing in intermittently connected mobile networks: the multiple-copy case," *IEEE/ACM Transactions on Networking*, vol. 16, no. 1, pp. 77–90, 2008.

[19] T. Spyropoulos, K. Psounis, and C. S. Raghavendra, "Efficient routing in intermittently connected mobile networks: the single-copy case," *IEEE/ACM Transactions on Networking*, vol. 16, no. 1, pp. 63–76, 2008.

[20] J. Leguay, T. Friedman, and V. Conan, "DTN routing in a mobility pattern space," in *Proceedings of ACM SIG-COMM Workshop on Computer Communications*, pp. 276–283, Philadelphia, Pa, USA, August 2005.

[21] H. Dubois-Ferriere, M. Grossglauser, and M. Vetterli, "Age matters: efficient route discovery in mobile ad hoc networks using encounter ages," in *Proceedings of the 4th ACM International Symposium on Mobile Ad Hoc Networking and Computing (MOBIHOC '03)*, pp. 257–266, June 2003.

[22] M. Shin, S. Hong, and I. Rhee, "DTN routing strategies using optimal search patterns," in *Proceedings of the Annual International Conference on Mobile Computing and Networking (MOBICOM '08)*, pp. 27–32, San Francisco, Calif, USA, September 2008.

[23] M. Quwaider and S. Biswas, "DTN routing in body sensor networks with dynamic postural partitioning," *Ad Hoc Networks*, vol. 8, no. 8, pp. 824–841, 2010.

[24] M. Quwaider and S. Biswas, "Probabilistic routing in on-body sensor networks with postural disconnections," in *Proceedings of the 7th ACM International Symposium on Mobility Management and Wireless Access (MobiWac '09)*, pp. 149–158, Tenerife, Spain, October 2009.

[25] C. Otto, A. Milenkovic, C. Sanders, and E. Jovanov, "System architecture of a wireless body area sensor network for ubiquitous health monitoring," *Journal of Mobile Multimedia*, vol. 1, pp. 307–326, 2006.

[26] B. Braem, B. Latré, I. Moerman, C. Blondia, and P. Demeester, "The wireless autonomous spanning tree protocol for multi-hop wireless body area networks," in *Proceedings of the 3rd Annual International Conference on Mobile and Ubiquitous Systems (MobiQuitous '06)*, July 2006.

[27] B. Latré, B. Braem, I. Moerman et al., "A low-delay protocol for multihop wireless body area networks," in *Proceedings of the 4th Annual International Conference on Mobile and Ubiquitous Systems: Computing, Networking and Services (MobiQuitous '07)*, August 2007.

[28] S. Jain, K. Fall, and R. Patra, "Routing in a delay tolerant network," in *Proceedings of the ACM SIGCOMM Conference*

on Applications, Technologies, Architectures, and Protocols for Computer Communications, pp. 145–157, 2004.

[29] A. Vahdat and D. Becker, "Epidemic routing for partially connected ad hoc networks," Tech. Rep. CS-200006, Duke University, 2000.

[30] P. Juang, H. Oki, Y. Wang, M. Martonosi, L.-S. Peh, and D. Rubenstein, "Energy-efficient computing for wildlife tracking: design tradeoffs and early experiences with ZebraNet," in *Proceedings of the 10th International Conference on Architectural Support for Programming Languages and Operating Systems*, pp. 96–107, October 2002.

[31] T. Spyropoulos, K. Psounis, and C. S. Raghavendra, "Spray and wait: An efficient routing scheme for intermittently connected mobile networks," in *Proceedings of the ACM SIGCOMM Workshop on Delay-Tolerant Networking (WDTN '05)*, pp. 252–259, 2005.

[32] S. Ni, Y. Tseng, Y. Chen, and J. Sheu, "The broadcast storm problem in a mobile ad hoc network," in *Proceedings of the 5th annual ACM/IEEE International Conference on Mobile Computing and Networking*, pp. 151–162, Seattle, Wash, USA, 1999.

[33] A. Jindal and K. Psounis, "Performance analysis of epidemic routing under contention," in *Proceedings of the 2006 International Wireless Communications and Mobile Computing Conference (IWCMC '06)*, pp. 539–544, Vancouver, Canada, July 2006.

[34] S. Burleigh, A. Hooke, L. Torgerson et al., "Delay-tolerant networking: an approach to interplanetary internet," *IEEE Communications Magazine*, vol. 41, no. 6, pp. 128–136, 2003.

[35] M. Quwaider and S. Biswas, "Probabilistic routing in on-body sensor networks with postural disconnections," in *Proceedings of the 7th ACM International Symposium on Mobility Management and Wireless Access (MobiWac'09)*, pp. 149–158, Tenerife, Spain, 2009.

[36] M. Quwaider and S. Biswas, "On-body packet routing algorithms for body sensor networks," in *Proceedings of the 1st International Conference on Networks and Communications (NetCoM '09)*, pp. 171–177, December 2009.